Chemically Driven Nanoscopic Magnetic Phase Separation at the $SrTiO_3(001)/La_{1-x}Sr_xCoO_3$ Interface

*Maria A. Torija, Manish Sharma, Jaume Gazquez, Maria Varela, Chunyong He, Josh Schmitt, Julie A. Borchers, Mark Laver, Sami El-Khatib, and Chris Leighton**

The remarkable functionality of perovskite oxides provides many opportunities for new physics, in addition to applications in solid oxide fuel cells, ferroelectric memory, and many other oxide electronic and spintronic devices.[1] The interface between a ferromagnetic- (FM) or metallic-doped perovskite (e.g., $La_{1-x}Sr_xMnO_3$ (LSMO)) and a non-magnetic insulator (e.g., $SrTiO_3$ (STO)) is a fundamental building block in such structures. Even such "simple" interfaces present significant challenges however, as exemplified by perovskite tunnel junctions. The high spin polarization of LSMO, and the lattice match to STO, suggest high tunneling magnetoresistance (TMR) in epitaxial LSMO/STO/LSMO junctions. Such high TMR has been realized at low temperature (T) but it drops precipitously as T increases,[2,3] an effect that was linked to thermal instability of the surface magnetization.[4] Maintaining high magnetization and Curie temperature (T_C) at such interfaces is in fact a significant challenge,[5,6] and even single manganite films grown on single crystal substrates display deterioration in the magnetoelectronic properties in the thin film limit.[7–9] The origin of these difficulties can be rationalized in terms of electronic phase competition. The wide range of ground states in systems such as manganites occurs due to close competition between the various degrees of freedom.[10] In addition to diversity in electronic properties, this competition results in magnetoelectronic phase separation (MEPS), where chemically homogeneous systems display spatial coexistence of multiple electronic or magnetic phases.[10] In heterostructures, interfacial effects like strain, electronic reconstruction, and charge transfer may perturb this competition,[7–9,11] making it difficult to maintain desired electronic properties close to interfaces with other oxides. Additionally, these oxides have complex chemistry and structure, which can be difficult to control at interfaces, particularly with regard to dopant concentration and O vacancies. The relative importance of these two classes of effects (i.e., electronic vs structural or chemical) is unclear.

Here, we approach this problem using $SrTiO_3(001)/La_{1-x}Sr_xCoO_3$. From the application viewpoint cobaltites are important for oxide fuel cells,[12,13] ferroelectric memories,[12,13] sensors,[12,13] catalysis,[13,14] and spintronics. In terms of basic science, LSCO is a good example of a FM metallic oxide. MEPS occurs at low x, with nanoscopic FM clusters forming in a non-FM insulating matrix.[15–17] As x is increased the clusters expand, percolating at $x_c = 0.18$, and forming a homogeneous FM metal at $x = 0.22$.[17] In the phase-separated regime an intercluster giant-magnetoresistance (GMR)-type effect occurs[16] due to spin-dependent intercluster transport. We find that these films exhibit a marked deterioration in magnetization and conductivity below some thickness, t^*. This is accompanied by MR of the intercluster GMR type, strong evidence of MEPS even at compositions that are homogeneous in bulk, with direct proof provided by small-angle neutron scattering (SANS) measurements. Scanning transmission electron microscopy (STEM) and electron energy loss spectroscopy (EELS) demonstrate that MEPS occurs due to nanoscale hole doping inhomogeneity near the interface, caused by depthwise variations in Sr and O, driven by simple thermodynamic and structural effects. These results show not only that the degradation in properties is due to MEPS, but that this is attributable purely to interfacial chemical phenomena.

STO(001)/LSCO epitaxial films (1.8% lattice mismatch, tensile strain) were deposited by high pressure reactive dc sputtering. Growth conditions and a comprehensive structural analysis at $x = 0.50$ have been reported previously.[18] The deposition rate was 0.9, 1.0, and 0.60 Å min^{-1} at $x = 0.50$, 0.28, and 0.22, respectively, and the films were deposited on untreated STO(001) substrates at 700 °C. Films grown on TiO_2-terminated STO(001) gave identical results. Magnetometry and magnetotransport (13.7 Hz, van der pauw) were measured from 5–300 K in in-plane fields to 9 T. Normal incidence SANS was

Dr. M. A. Torija, Dr. M. Sharma, Dr. C. He, J. Schmitt, Dr. S. El-Khatib, Prof. C. Leighton
Department of Chemical Engineering and Materials Science
University of Minnesota
Minneapolis, MN 55455, USA
E-mail: leighton@umn.edu
Dr. J. Gazquez, Dr. M. Varela
GFMC, Dept. Fisica Aplicada III
Universidad Complutense de Madrid. Madrid, 28040, Spain
Dr. J. Gazquez, Dr. M. Varela
Materials Science and Technology Division
Oak Ridge National Laboratory
Oak Ridge, TN 37831, USA
Dr. J. A. Borchers, Dr. M. Laver
NIST Center for Neutron Research
National Institute for Standards and Technology
Gaithersburg, MD 20899, USA
Dr. S. El-Khatib
NIST Center for Neutron Research
National Institute for Standards and Technology
Gaithersburg, MD 20899, USA
Prof. S. El-Khatib
Department of Physics
American University of Sharjah
PO Box 26666, Sharjah, United Arab Emirates

DOI: 10.1002/adma.201100417

ADVANCED MATERIALS
www.advmat.de

www.MaterialsViews.com

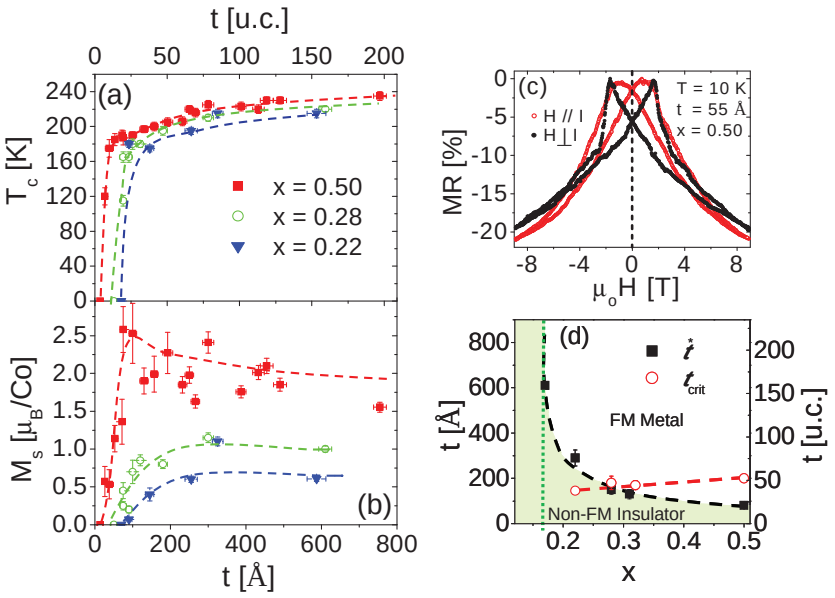

Figure 1. Thickness dependence of a) the Curie temperature and b) the 10 K saturation magnetization for films with $x = 0.50$, 0.28, and 0.22. Dashed lines are guides for the eye. c) Field dependence of the magnetoresistance of a 55 Å thick $x = 0.5$ film at 10 K in both field orientations. d) Doping dependence of t^* and the critical thickness for strain relaxation. The vertical dotted line marks x_c.

carried out at the NIST Center for Neutron Research at a wavelength of 5 Å, in the wave vector range 0.006 Å^{-1} < q < 0.2 Å^{-1}. Triply stacked 1-in. diameter samples were employed, and absolute cross-sections containing both magnetic and structural film scattering were determined via careful background subtraction on prescreened substrates. STEM-EELS was performed along a [100] pseudocubic zone axis in an aberration-corrected VG Microscopes HB501UX (100 kV), equipped with an Enfina EEL spectrometer.[19] Powder samples were crushed and dispersed on a holey C film, while film specimens were prepared by conventional methods (grinding, dimpling, and Ar ion milling).

The degradation in magnetic properties at low thickness (t), qualitatively similar to that seen in many complex oxides, is shown in **Figure 1**a,b for $x = 0.50$, 0.28, and 0.22, i.e., the homogeneous FM metallic phase in bulk. Starting at $x = 0.50$, we observe a gradual decrease in T_C[20,21] to ≈30 Å, followed by a rapid decrease at lower t. The saturation magnetization (M_S) is slightly different. M_S lies around the bulk value (1.92 μ_B Co^{-1}[15]) for $t \geq 100$ Å then decreases rapidly between 100 and 72 Å. We thus identify a thickness, t^* (≈80 Å in this case), where M_S is significantly suppressed, while T_C remains high, around 190 K. As x is decreased the low t degradation becomes more pronounced, to the point where M_S begins to fall at t values as high as 300 Å for $x = 0.22$. As discussed in detail in the Supporting Information (including Figure S1), the T dependent resistivity (ρ), measured as a function of t and x, reveals that the suppression of M_S is accompanied by a crossover from metallic-like ($d\rho/dT > 0$), to insulating-like ($d\rho/dT < 0$) behavior. From extensive $M_S(t)$ and $\rho(T,t)$ data we find $t^* = 80$ Å at $x = 0.50$, increasing to 150 Å at $x = 0.28$ and 300 Å at $x = 0.22$. More importantly, the crossover to a suppressed M_S state with $d\rho/dT < 0$ is accompanied by the onset of large MR at low T (see Supporting Information, Figure S1). Figure 1c shows the field (H) dependence of this MR for $x = 0.5$, $t = 55$ Å, and $T = 10$ K. The similarity between this MR in heavily doped LSCO at low t, and the intercluster "GMR" in low doped bulk crystals[16] is striking. Given the large magnitude, the sign, the H and T dependence, the hysteresis (with peaks in $\rho(H)$ at the coercive field), and the isotropy with respect to current and H directions (eliminating conventional anisotropic MR), we conclude that below t^*, these high x films exhibit intercluster MR. The obvious implication is that they are magnetically phase separated on a nanoscopic scale. We conclude that in films with $t < t^*(x)$, or in the region within $t^*(x)$ of the interface in thicker films, isolated nanoscopic FM clusters form in an insulating non-FM matrix, explaining the suppressed M_S and insulating $\rho(T)$. At even lower t, when the isolated cluster FM becomes thermally unstable, T_C drops quickly (Figure 1b). The MEPS in the very thin film limit is similar to that seen in STO(001)/$La_{2/3}Ca_{1/3}MnO_3$ (LCMO) by NMR,[7] although in this case the intercluster "GMR" considerably simplifies detection.

It is important to consider structural effects that could drive the crossover at t^*. In this regard we make two observations. First, the coalescence thickness (≈25 Å) lies well below t^*, even at $x = 0.50$.[18] At lower x, where $t^* \approx 300$ Å, this is beyond doubt. Second, the suppressed M_S state below t^* cannot be ascribed solely to strain. At $x = 0.50$, reciprocal space maps reveal fully strained pseudomorphic films below a critical thickness for strain relaxation (t_{crit}) of ≈200 Å.[18] Films with $t < 200$ Å are thus in an identical strain state, meaning that the crossover at $t^* = 80$ Å cannot be driven by strain alone. In fact, we find no significant variation in structural parameters below 200 Å. This general point is emphasized in Figure 1d, which displays $t^*(x)$ and $t_{crit}(x)$. t_{crit} exhibits the expected weak x dependence, while t^* diverges as $x \rightarrow x_c^+$. There is no similarity between t^* and t_{crit}, either in magnitude or x dependence, demonstrating that the low M_S insulating state is not purely strain driven.

Direct proof of nanoscopic MEPS was obtained from SANS on 650 Å, $x = 0.50$ films. The T dependence of the film scattering cross-section ($d\Sigma/d\Omega$) is shown in **Figure 2** at q = 0.007 Å^{-1} (length scale of ≈900 Å) and $q = 0.075$ Å^{-1} (≈80 Å). The low q $d\Sigma/d\Omega$ turns on at T_C, confirming long-range FM order. At low T, $d\Sigma/d\Omega(q)$ is of the Porod type, due to scattering from FM domains in excess of 1000 Å (see Supporting Information and Figure S2). The high q $d\Sigma/d\Omega$ indicates that these films do not present pure long-range FM order however. Although the usual critical scattering is observed around T_C (likely in addition to T-independent film structural scattering), the high q $d\Sigma/d\Omega$ does not vanish as $T \rightarrow 0$. In contrast to expectations for long-range FM,[17] the high q $d\Sigma/d\Omega$ is finite at low T (note the scale), and even exhibits an upturn at the lowest T. Although $d\Sigma/d\Omega$ in this q range is too noisy to allow a fit to a specific functional form to extract the correlation length,[17] the observation of finite and strongly T-dependent high q intensity as $T \rightarrow 0$ is

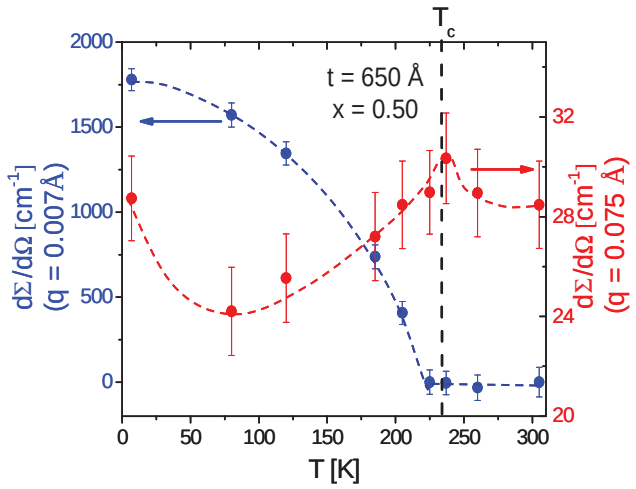

Figure 2. Temperature dependence of the SANS cross section (averaged over 3 adjacent q points) at $q = 0.007$ (left axis) and 0.075 Å^{-1} (right axis) for an $x = 0.50$, 650 Å film. Dashed lines are guides for the eye.

evidence of short-range FM on the 10–100 Å scale. Given the data in Figure 1, we deduce that these FM clusters are located near the STO interface.

Having established MEPS as the origin of degraded magnetism and transport, cross-sectional STEM/EELS was used to assess possible depthwise variations in chemistry and electronic structure. The atomic resolution Z-contrast STEM image (**Figure 3**a), shows a sharp, coherent interface. In order to use the EELS O K edge as a local probe of Co–O bonding, bulk powders ($0.00 \le x \le 0.50$)[15] were used as calibration standards. Additional detail on the EELS analysis is provided in the Supporting Information. Their O K edge spectra (normalized to the 535 eV main peak) are shown in Figure 3b, focusing on the pre-peak near 527 eV, which can be decomposed into two peaks at 527 and 529 eV due to O 2p holes and Co–O hybridization.[22,23] The intensity of the O 2p hole contribution, normalized to the 535 eV main peak, is plotted versus x in Figure 3b, providing a means to map the local hole doping. Figure 3d shows such a spectral map, acquired in the region shown in Figure 3c on a 450 Å film. The level of inhomogeneity, both laterally and depthwise, is striking. The obvious depletion in hole density within 10 nm of the interface is highlighted in Figure 3e, where the laterally averaged peak intensity is plotted versus depth. At the interface the intensity falls to 0.104, corresponding (Figure 3b) to an effective doping level, $x_{eff} \approx 0.23$. To determine if this suppression is driven by chemical variations, O K and Sr $L_{2,3}$ edge maps were acquired in the same region

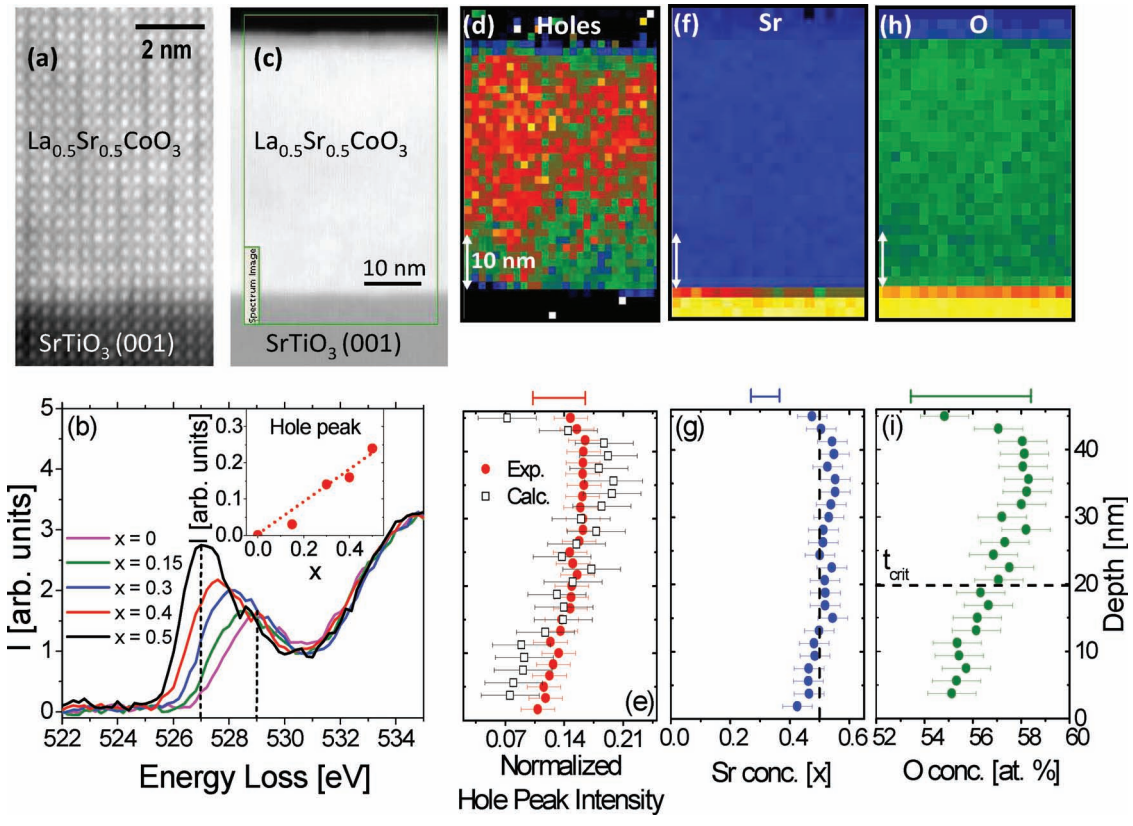

Figure 3. a) High-resolution Z-contrast STEM image of the interface region in a 450 Å thick $x = 0.50$ film. b) Normalized bulk EELS spectra at $x =$ 0.00, 0.15, 0.30, 0.40, and 0.50 in the vicinity of the O K edge. Inset: Doping dependence of the normalized hole peak intensity (with straight line fit). c) Low-magnification image of the same film. The rectangle marks the region where EELS images were acquired. Panels (d,f,h) show the derived images, while panels (e,g,i) show laterally averaged depth profiles. In (e) the open points are calculated from (g) and (i), as described in the text. Error bars indicate relative random errors. The large bar at the top of plots (e,g,i) indicates the systematic error.

(Figure 3f,h). Lateral averaging produces the depth-profiles shown in Figure 3g,i, showing that subtle variations in Sr and O content exist, as in STO(001)/LCMO.[24] Figure 3g shows that the Sr doping actually exceeds 0.5 in the bulk of the film, but is reduced within ≈10 nm of the interface, reaching as low as 0.42. While significant, this is insufficient to explain effective hole doping of only 0.23. However, Figure 3i shows that the O content also exhibits depthwise variation, decreasing by 3% as the interface is approached. Although the systematic errors (see figure and caption) preclude accurate absolute O content determination, the relative errors are smaller. Assuming the peak O content actually corresponds to close to full oxygenation (based on bulk-like properties at high t), this 3% decrease corresponds to 2.91 O ions per unit cell. Combining this with the Sr data, we deduce that these nominally $x = 0.5$ films have composition $La_{0.58}Sr_{0.42}CoO_{2.91}$ at the interface, an effective doping ($x_{eff} = x - 2\delta$, where δ is the oxygen defficiency) of only 0.24. The remarkable agreement with the value from the normalized hole peak intensity (0.23) demonstrates that the reduction in interfacial hole density is completely accounted for by the combined effects of Sr and O content. This holds for the entire depth profile, as shown by the open points in Figure 3e, which are reconstructed from the Sr and O data (Figure 3g,i), using the inset to Figure 3b to relate x_{eff} at each depth to the hole peak intensity.

The significance of this result is immediately clear; the depthwise variations in Sr and O lead to an effective interfacial doping level (0.24) well below the nominal value (0.5). The interface hole doping value is in fact very close to that at which MEPS emerges in bulk (x = 0.22[17]), sufficiently so that even minor additional disorder will favor the phase-separated state. We thus conclude that the interfacial MEPS is driven by chemical effects, which lower the local hole doping to a level where MEPS is expected,[17] with no need to invoke charge transfer or electronic reconstructions. These results also provide a simple explanation for the form of $t^*(x)$ (Figure 1d); the decrease in Sr and O content near the interface has an increasingly dramatic effect at lower nominal x, as $x \rightarrow x_c^+$. Clearly, the outstanding issue is the origin of these compositional variations. Although experimental data is scarce, diffusion of Sr (Ca) towards the surface has been reported in LSMO (LCMO) over a wide range of conditions.[24–26] With the exception of the topmost surface region, which may be susceptible to artifacts in STEM/EELS, this is broadly consistent with our data (Figure 3g). The atomistic defect chemistry simulations of Read et al.[27] are also relevant. They find that the energy required to dissolve Sr in $LaCoO_3$ via a hole doping/Co^{4+} mechanism is 3.21 eV on the (001) surface cf. 2.42 eV in the bulk. It is thus favorable for Sr dissolution via this mechanism to occur in the film interior, consistent with Figure 3g. Note however that charge balance via O vacancy formation or O hole doping are also possible, and the competition between these mechanisms is likely subtle and x-dependent. Additional computational and experimental work in this area would be valuable. In terms of the oxygen depth profile, it is likely that epitaxial strain plays a role. It has been suggested that in thin-film perovskites such as LSCO tensile strain favors O deficiency, and the link between strain state and O vacancies is provided by O vacancy ordering.[28] It is thus possible that the increase in O content above about 100–200 Å from the STO(001) interface (Figure 3j) is linked to strain relaxation, and the agreement with the experimental t_{crit} is quite reasonable. Both of these explanations suggest that the depletion of holes near the interface is intrinsic to the STO(001)/LSCO system.

In summary, the degradation in magnetic and electronic properties of metallic perovksites in the very thin-film limit has been studied in detail in $SrTiO_3(001)/La_{1-x}Sr_xCoO_3$. We find that nanoscopic interfacial magnetoelectronic phase separation is responsible. This occurs due to nanoscale inhomogeneity in hole doping near the interface, driven by depthwise variations in Sr and O content, which can be rationalized in terms of thermodynamic and structural arguments. The deterioration in properties is thus driven by chemical, rather than electronic, effects.

Supporting Information

Supporting Information is available from the Wiley Online Library or from the author.

Acknowledgements

Work at UMN was supported by NSF (DMR-0804432) and DoE (DE-FG02–06ER46275, neutron scattering). Work at ORNL (MV) was supported by the US DoE, Office of Basic Energy Sciences, Materials Sciences and Engineering Division. J.G. acknowledges the Spanish MEC 2007–0086 and the European Research Council Starting Investigator Award. The authors are grateful to J.T. Luck for STEM specimen preparation and B.B. Maranville for SANS assistance.

Received: February 2, 2011
Published online: April 20, 2011

[1] R. Ramesh, D. G. Schlom, *MRS Bull.* **2008**, *33*, 1006.
[2] A. Gupta, J. Z. Sun, *J. Mag. Magn. Mater.* **1999**, *200*, 24.
[3] M. Bowen, M. Bibes, A. Barthelemy, J. P. Contour, A. Anane, Y. Lemaitre, A. Fert, *Appl. Phys. Lett.* **2003**, *82*, 233.
[4] J.-H. Park, E. Vescovo, H.-J. Kim, C. Kwon, R. Ramesh, T. Venkatesan, *Phys. Rev. Lett.* **1998**, *81*, 1953.
[5] V. Garcia, M. Bibes, A. Barthelemy, M. Bowen, E. Jacquet, J.-P. Contour, A. Fert, *Phys. Rev. B.* **2004**, *69*, 052403.
[6] J. J. Kavich, M. P. Warusawithana, J. W. Freeland, P. Ryan, X. Zhai, R. H. Kodama, J. N. Eckstein, *Phys. Rev. B.* **2007**, *76*, 014410.
[7] M. Bibes, L. Balcells, S. Valencia, J. Fontcuberta, M. Wojcik, E. Jedryka, S. Nadolski, *Phys. Rev. Lett.* **2001**, *87*, 067210.
[8] M. Hujiben, L. W. Martin, Y.-H. Chu, M. B. Holcomb, P. Yu, G. Rijnders, D. H. A. Blank, R. Ramesh, *Phys. Rev. B.* **2008**, *78*, 094413.
[9] R. V. Chopdekar, E. Arenholz, Y. Suzuki, *Phys. Rev. B.* **2009**, *79*, 104417.
[10] E. Dagotto, *Nanoscale phase separation and colossal magnetoresistance*, Springer, New York **2002**.
[11] S. Smadici, P. Abbamonte, A. Bhattacharya, X. Zhai, B. Jiang, A. Rusydi, J. N. Eckstein, S. D. Bader, J.-M. Zuo, *Phys. Rev. Lett.* **2007**, *99*, 196404.
[12] S. Madhukar, S. Aggarwal, A. M. Dhote, R. Ramesh, A. Krishnan, D. Keeble, E. Poindexter, *J. Appl. Phys.* **1997**, *81*, 3543.
[13] L. Malavasi, E. Quartarone, C. Sanna, N. Lampis, A. G. Lehmann, C. Tealdi, M. C. Mozzati, G. Flor, *Chem. Mater.* **2006**, *18*, 5230.
[14] C. H. Kim, G. Qi, K. Dahlberg, W. Li, *Science* **2010**, *327*, 1624.
[15] J. Wu, C. Leighton, *Phys. Rev. B.* **2003**, *67*, 174408.

[16] J. Wu, J. W. Lynn, C. Glinka, J. Burley, H. Zheng, J. F. Mitchell, C. Leighton, *Phys. Rev. Lett.* **2005**, *94*, 037201.
[17] C. He, S. El-Khatib, J. Wu, J. W. Lynn, H. Zheng, J. F. Mitchell, C. Leighton, *Europhys. Lett.* **2009**, *87*, 27006.
[18] M. A. Torija, M. Sharma, M. R. Fitzsimmons, M. Varela, J. Wu, C. Leighton, *J. Appl. Phys.* **2008**, *104*, 023901.
[19] Identification of a commercial product or trade name does not imply endorsement or recommendation by NIST.
[20] D. Fuchs, T. Schwarz, O. Moran, P. Schweiss, R. Schneider, *Phys. Rev. B.* **2005**, *71*, 092406.
[21] C. Xie, J. I. Budnick, B. O. Wells, J. C. Woicik, *Appl. Phys. Lett.* **2007**, *91*, 172509.
[22] A. R. Moodenbaugh, B. Nielsen, S. Sambasivan, D. A. Fischer, T. Friessnegg, S. Aggarwal, R. Ramesh, R. L. Pfeffer, *Phys. Rev. B.* **2000**, *61*, 5666.
[23] M. Abbate, J. C. Fuggle, A. Fujimori, L. H. Tjeng, C. T. Chen, R. Potze, G. A. Sawatzky, H. Eisaki, S. Uchida, *Phys. Rev. B.* **1993**, *47*, 16124.
[24] S. Estrade, J. Arbiol, F. Peiro, I. C. Infante, F. Sanchez, J. Fontcuberta, F. de la Pena, M. Walls, C. Colliex, *Appl. Phys. Lett.* **2008**, *93*, 112505.
[25] R. Bertacco, J. P. Contour, A. Barthelemy, J. Olivier, *Surf. Sci.* **2002**, *511*, 366.
[26] T. T. Fister, D. D. Fong, J. A. Eastman, P. M. Baldo, M. J. Highland, P. H. Fuoss, K. R. Balasubramanian, J. C. Meador, P. A. Salvador, *Appl. Phys. Lett.* **2008**, *93*, 151904.
[27] M. S. D. Read, M. S. Islam, G. W. Watson, F. King, F. E. Hancock, *J. Mater. Chem.* **2000**, *10*, 2298.
[28] D. O. Klenov, W. Donner, B. Foran, S. Stemmer, *Appl. Phys. Lett.* **2003**, *82*, 3427.